Resonant two-photon transition to the continuum from an initial $J=0$ state using elliptically polarized light

Banani Datta and S. S. Bhattacharyya
Atomic and Molecular Physics Section, Department of Materials Science, Indian Association for the Cultivation of Science, Calcutta 700 032, India

(Received 3 September 1993; revised manuscript received 25 May 1994)

We have studied the transition probabilities and the photofragment energy and angular distributions in a resonant two-photon transition to the continuum with an elliptically polarized radiation field. The general formalism applies both to ionization of atoms within the framework of a single-electron model and the dissociation of diatomic molecules with the involvement of Σ states only. Detailed calculations for an initial $J=0$ state give the observable quantities as functions of detuning, intensity, and the polarization parameter for several combinations of the system parameters such as bound-bound and bound-continuum couplings and the Fano q parameter. For sufficiently intense fields the Raman-like coupling between the two coherently excited magnetic sublevels of the resonant $J=1$ state (one of which can be decoupled from the ground state by a linear transformation) causes a significant enhancement of the transition probability near the Fano minimum obtained for linearly or circularly polarized fields. The evolution of the photofragment kinetic-energy distribution changes with the ellipticity parameter of the radiation. The angular distribution becomes intensity dependent for general ellipticity parameters; the shapes of the resultant distribution in different space-fixed planes are discussed.

PACS number(s): 33.80.Rv, 33.80.Wz

INTRODUCTION

Resonance-enhanced intense-field multiphoton transitions to the continuum of an atomic or molecular system has been extensively studied in the past few years [1]. Generally, in such transitions, a set of degenerate or near-degenerate field plus atom-molecule levels is coherently excited by the resonance absorption. The characteristics of the transition to the continuum then depends upon the symmetry properties and excitation process of this set of coherently excited resonant levels [2]. In intense electromagnetic field, however, the set of energy levels dressed by the radiation field, rather than the unperturbed levels, determines these characteristics. The eigenvalues, wave functions, and symmetry properties of the bound states are modified from the field-free values. This is the reason why theoretical studies of resonance-enhanced multiphoton transitions to the continuum are of fundamental interest. Such studies, when combined with the proper experiments, may help to advance our understanding of the fundamental aspects of radiation-matter interaction.

The symmetry properties of such resonantly excited dressed states will of course depend on the polarization of the incident radiation. Absorption of polarized radiation transfers population to a group of oriented and/or aligned intermediate states undergoing radiative transitions to the continuum [3]. In a strong field with the involvement of many radiatively coupled states, the polarization dependence affects the characteristics of the phenomenon concerned in a strongly nonlinear way [4].

The polarization dependence of weak-field two-photon processes with a single intermediate resonance has already been investigated by a number of authors [3,5]. The polarization dependence of the photoelectron angular distribution in resonant atomic multiphoton ionization when two closely spaced resonant fine-structure levels are excited has been shown to require detailed computation and is not predictable from general considerations [6]. Most of the studies reported so far have used linearly or circularly polarized light.

For elliptically polarized light, with the propagation direction of the radiation as the space-fixed Z axis, each magnetic sublevel m of an initial state with well-defined angular momentum J will be coherently coupled to two magnetic sublevels $m\pm1$ of the resonant state. The different magnetic substates of the initial and resonant states will be differently shifted and broadened by the elliptically polarized field [7]. Each magnetic sublevel m will be nonlinearly coupled to $m\pm2$ states of the same manifold through real and imaginary parts of Raman-like couplings [8]. The excitation process can be broken down into two independent ladders, one consisting of all odd m sublevels of the initial state and even m sublevels of the resonant state. The other ladder will have the odd and even m sublevels interchanged between the initial and resonant states. The dynamics of such a system can be very complicated in near-resonance intense fields causing important modifications in the transition rates, probabilities, and angular distribution of photofragments of the atom-molecule system from that in cases of linear or circular polarizations. So far there have been very few studies on resonant interactions of atoms and molecules with strong elliptically polarized fields and, as far as we know, none on the effects of elliptical polarization on features of continuum transitions. However, recently a formulation has been presented for formation of coherent stationary states of an atom in interaction with elliptically polarized

resonant light in a magnetic field [9]. This study also stresses the unequal distribution among the magnetic sublevels arising from the coherent excitation of the different magnetic sublevels of the resonant state. However, in the present study we are not concerned with the property of those stationary states as such, but rather with the behavior of an unpolarized initial state.

The angular distributions of the two-photon ionization or dissociation fragments and their dependence on the polarization and intensity can be very interesting in the presence of such mutual couplings between m states with some of the couplings varying nonlinearly with field. The angular distribution now will characterize the rotational properties of the mixed state at different intensities.

In this work the resonant two-photon transition probabilities and the kinetic-energy distribution of the photofragments in the continuum, as well as their angular distribution, have been obtained in an elliptically polarized field as functions of its intensity, frequency, and polarization parameter in the presence of a background of nonresonant bound and continuum states with allowed dipole transitions. After giving the general formulation detailed calculations have been presented only for the special case of transition from an initial $J=0$ state through a $J=1$ resonant level within the framework of the resolvent operator formalism [10]. The various observable quantities mentioned above have been obtained in terms of three parameters, the bound-bound coupling, the width of the resonant state, and the Fano asymmetry parameter defined as usual for linearly polarized radiation. We have concentrated on different cases where the bound-bound coupling is much weaker compared to the bound-continuum coupling and when the two are of the same order. Realistic values of the Fano asymmetry parameter have been assumed. It may be mentioned here that the formulation will be applicable both to atomic ionization within the framework of the one-electron picture and to molecular photodissociation through an electronically excited intermediate resonance provided all the relevant molecular states are Σ states and no other molecular frame quantum numbers arise. We also neglect electronic spin.

FORMULATION

The interaction Hamiltonian between an atomic or molecular system and a monochromatic elliptically polarized electromagnetic field of angular frequency ω propagating along the space-fixed Z axis can be represented as

$$\hat{V}=-i\left[\frac{2\pi\omega}{V}\right]^{1/2}\left[\left\{-A\sum_{\lambda}D^{1*}_{1\lambda}d_{\lambda}+B\sum_{\lambda}D^{1*}_{-1\lambda}d_{\lambda}\right\}\hat{a}+\left\{A^{*}\sum_{\lambda}D^{1*}_{-1\lambda}d_{\lambda}-B^{*}\sum_{\lambda}D^{1*}_{1\lambda}d_{\lambda}\right\}\hat{a}^{\dagger}\right], \tag{1}$$

where $d_0=d_z$, $d_{\pm1}=(1/\sqrt{2})(d_x\pm id_y)$, and d_x, d_y, and d_z are the body-fixed components of the transition dipole moment operator $\mathbf{d}$. The coefficients A and B are

$$A=\cos\left[\phi+\frac{\pi}{4}\right]e^{-i\psi}, \tag{2a}$$

$$B=\sin\left[\phi+\frac{\pi}{4}\right]e^{i\psi}, \tag{2b}$$

where

$$\tan\phi=\frac{b}{a}. \tag{2c}$$

Here ψ is the angle between the major axis of the ellipse and the space-fixed X axis. a and b are the lengths of the major and minor axes, respectively, of the field ellipse [11]. Equation (1) represents a coherent superposition of the operators corresponding to right and left circularly polarized radiation with different coefficients. The corresponding interaction Hamiltonian then contains terms causing absorption and emission of both the circularly polarized components with the selection rules $\Delta M=\pm1$ in both absorption and emission, where M is the component of the angular momentum J along the propagation direction Z. The operators corresponding to the transition $\Delta M=\pm1$ enter V with different coefficients in absorption and emission.

Let the initial state of the system be $|G,J_g,M_g\rangle$. By absorption of a single photon of frequency ω the system can be resonantly excited to a coherent superposition of states $|A,J_a,M_g+1\rangle$ and $|A,J_a,M_g-1\rangle$, with the angular momentum of the resonant state J_a equal to either J_g+1 or J_g-1. These two states will be Raman coupled to each other through the continuum and discrete states and radiatively coupled also to $|G,J_g,M_g+2\rangle$ and $|G,J_g,M_g-2\rangle$, respectively, and so on. For consideration of all such couplings let us define a projection operator P (and $Q=1-P$) in the space of the $(2J_g+1)+(2J_a+1)$ field molecule states with the basis $|g_{M_g}\rangle=|G,J_g,M_g\rangle|n\rangle$ and $|a_{M_a}\rangle=|A,J_a,M_a\rangle|n-1\rangle$, where $|n\rangle$, etc. are the photon number states [12],

$$P=\sum_{k=-J_g}^{J_g}|g_k\rangle\langle g_k|+\sum_{l=-J_a}^{J_a}|a_l\rangle\langle a_l|. \tag{3}$$

Now, considering the definition of the resolvent operator

$$G(z)=\frac{1}{z-H},\quad G_0(z)=\frac{1}{z-H_0}, \tag{4}$$

where

$$H=H_M+H_F+V=H_0+V \tag{5}$$

and H_M and H_F are the molecular and radiation field Hamiltonians, respectively, coupled equations satisfied by the matrix elements of G in the P space obtained for the initial state $|g_\alpha\rangle$ can be written as

$$(z-E_{g_\alpha}-R_{g_\alpha,g_\alpha})G_{g_\alpha,g_\alpha}-\sum_{k}R_{g_\alpha,g_k}G_{g_k,g_\alpha}-\sum_{l}R_{g_\alpha,a_l}G_{a_l,g_\alpha}=1 \tag{6a}$$

$$(z-E_{g_k})G_{g_k,g_\alpha}-\sum_{k'}R_{g_k,g_{k'}}G_{g_{k'},g_\alpha}-\sum_{l}R_{g_k,a_l}G_{a_l,g_\alpha}=0\ ,$$

$$k=-J_g \text{ to } J_g \qquad (6b)$$

$$(z-E_{a_l})G_{a_l,g_\alpha}-\sum_{k}R_{a_l,g_k}G_{g_k,g_\alpha}-\sum_{l'}R_{a_l,a_{l'}}G_{a_{l'},g_\alpha}=0\ ,$$

$$l=-J_a,\ldots,J_a. \qquad (6c)$$

where $l=-J_a,\ldots,J_a$ and R is the shift operator given by

$$R=R(E_g),\quad R(z)=V+\sum_{k=1}^{\infty}[V(QG_0QV)]^k\ . \qquad (7)$$

Solutions of Eqs. (6) give $G_{g_i\alpha}$ and $G_{a_k\alpha}$ in terms of the matrix elements of R. Evaluation of the matrix elements of the shift operator R finally provides the parameters needed for the calculation of the probability of transition to the continuum. The real and imaginary parts of the infinite series associated with each of the R matrices will be evaluated to the lowest nonvanishing order in the rotating-wave approximation (RWA).

Thus we can write

$$R_{g_m,g_n}=\sum_i T^{(i)}_{g_m,g_n}(E_g)\ . \qquad (8)$$

Since a $|g\rangle$ to $|g\rangle$ transition must involve an even number of photons, $T^{(i)}$ for odd values of i give zero. The term $T^{(2)}$ can be expressed as

$$T^{(2)}_{g_m,g_n}(E_g)=\sum_{b_1,b_2}(V)_{g_m,b_1}\langle b_1|QG_0Q|b_2\rangle(V)_{b_2,g_n}. \qquad (9)$$

QG_0Q is diagonal in the basis of eigenfunctions of H_0 and assuming $|G\rangle$ to be the ground electronic state, in the RWA b_1 and b_2 must be states denoted by $|B_i\rangle|n-1\rangle$, where $|B_i\rangle$ are nonresonant discrete and continuum states

$$T^{(2)}_{g_m,g_n}(E_g)=\sum\int\frac{(V)_{g_m,b}(V)_{b,g_n}}{E_G+\hbar\omega-E_B}db=f_{g_m,g_n}\ . \qquad (10)$$

Thus the lowest-order contribution to the real parts of the matrix element of R between states of the g manifold occurs in the second order. The diagonal matrix elements give the energy shift of each g state due to single-photon virtual transitions from ground to nonresonant states and the nondiagonal matrix elements give the Raman coupling between different states.

Real parts of the fourth-order terms $T^{(4)}_{g_m,g_n}(E_g)$ in the expansion of diagonal matrix elements R_{g_m,g_m} give the shifts of the g_m states due to virtual two-photon transitions and the off-diagonal elements in the g manifold give the four-photon couplings. Since the shifts of these states and the real Raman couplings between them occur in second order also, the higher-order shifts and couplings need not be considered. However, because of the presence of an intermediate two-photon resonance in the continuum, each of the matrix elements in (8) will acquire an imaginary part in the fourth order. The diagonal imaginary terms will define the width of each g state due to two-photon transition to the continuum.

Thus we can write

$$R_{g_m,g_n}=f_{g_m,g_n}-(i/2)\gamma_{g_m,g_n}\ , \qquad (11)$$

where

$$\gamma_{g_m,g_n}=2\pi\sum_i V^{(2)}_{g_m,c_i}V^{(2)}_{c_i,g_n}\ . \qquad (12)$$

In a similar fashion

$$R_{a_m,a_n}=F_{a_m,a_n}-(i/2)\Gamma_{a_m,a_n}\ . \qquad (13)$$

Since from a level in the manifold a, there will be a single photon resonance in the continuum, both the real and imaginary terms arise from the second-order term in the expansion of R,

$$F_{a_m,a_n}=\sum_i \mathrm{P}\int\frac{(V)_{a_m,c_i}(V)_{c_i,a_n}}{E_G+\hbar\omega-E_B}dE_{c_i}. \qquad (14)$$

P denotes the principal value and

$$\Gamma_{a_m,a_n}=2\pi\sum_i(V_{a_m,c_i}V_{c_i,a_n})_{E_{c_i}=E_A+\hbar\omega}\ . \qquad (15)$$

Once again, the diagonal elements give the single-photon shifts and widths of the resonant state levels while the nondiagonal terms give the complex Raman couplings between the levels in the a manifold. In Eq. (14) the summation over all possible nonresonant discrete states satisfying the proper selection rules should be included. Also, Eqs. (12), (14) and (15) all involve summation over an index i, which distinguishes the different continua to which transitions may, in general, take place (e.g., continua with two different J values).

The real and imaginary parts of the matrix elements between the states in the g and a manifolds will arise from the first- and third-order terms, respectively, in the expansion of $R_{g,a}(E_g)$,

$$\begin{aligned}R_{g_m,a_n}(E_g)&=V_{g_m,a_n}+\sum_{j_1j_2}V_{g,j_1}\frac{1}{E_A+\hbar\omega-E_{j_1}}\\&\quad\times V_{j_1,j_2}\frac{1}{E_A+2\hbar\omega-E_{j_2}}V_{j_2,a_n}\\&=V_{g_m,a_n}+\sum_j\frac{V^{(2)}_{g_m,j}V_{j,a_n}}{E_G+2\hbar\omega-E_j}\\&=\bar V_{g_m,a_n}[1-i/q_{m,n}]\ ,\end{aligned} \qquad (16)$$

where

$$\bar V=V_{g_m,a_n}+\mathrm{P}\int\sum_l\frac{V^{(2)}_{g_m,c_i}V_{c_i,a_n}}{E_G+2\hbar\omega-E_{c_i}}dE_i \qquad (17)$$

and

$$1/q_{mn}=\pi\frac{\sum_l|V^{(1)}_{g_m,c_i}V_{c_i,a_n}|_{E_{c_i}=E_G+2\hbar\omega}}{\bar V_{g_m,a_n}}\ . \qquad (18)$$

$V^{(2)}_{g_m,c_i}$ is the usual two-photon matrix element for the continuum transition and $q_{m,n}$ is the effective asymmetry

parameter for coupling between g_m and a_n.

The evolution operator U is obtained as the Laplace transform of G,

$$U(t,0)=-\frac{1}{2\pi i}\int G(z)e^{-izt}dz \ . \tag{19}$$

In terms of the matrix elements of U the expression of transition probability to the continuum $P_\alpha(t)$ is obtained as

$$P_\alpha(t)=1-\sum_m |U_{g_m g_\alpha}(t)|^2-\sum_n |U_{a_n g_\alpha}(t)|^2 \ . \tag{20}$$

The contributions to the various matrix elements of U arise from the poles of the corresponding matrix elements of G below the real axis which, as usual, are given by the roots of the secular equation arising from the system of linear equations (6). The expression for the photofragment spectra at a continuum energy ε is obtained as

$$W(\varepsilon,t)=(2J_g+1)^{-1}\sum_{g_\alpha}\sum_i |U_{c_i g_\alpha}(\varepsilon,t)|^2 \ . \tag{21}$$

Thus, in principle, all that remains is to determine the matrix elements of V between different states and use them to get the matrix elements of R to various orders.

As stated above, we neglect all angular momentum couplings such as the molecular frame angular momentum quantum numbers or the electronic spin angular momentum and consider only the changes in the orbital angular momentum quantum number. Thus the formalism can be applied to atomic two-photon photoionization within the framework of a simple one-electron model or to two-photon dissociation of diatomic molecules through the involvement of Σ states only with the neglect of electron-spin quantum numbers. Within this limitation the bound- and continuum-state wave functions for the diatomic molecular case using the Born-Oppenheimer approximation can be generally written as [3]

$$\Psi_{\text{bound}}=[(2J+1)/4\pi]^{1/2}R_{vJ}(r)\Psi_e(r_e,r)D^J_{M0}(\phi,\theta,0) \ , \tag{22a}$$

$$\Psi_{\text{free}}=(1/4\pi)\sum_{J,M}(2J+1)(i)^J\exp(-i\delta_J)R_{kJ}(r) \times D^J_{M0}(\phi,\theta,0) \times D^J_{M0}(\phi_k,\theta_k,0)\Psi_e(r_e,r) \ . \tag{22b}$$

Here r_e collectively denotes the coordinates of all electrons and r is the internuclear separation. θ and ϕ are the orientations of the internuclear axis in the space-fixed frame. In the atomic case the general form of the wave functions will be similar, but the radial part will be a function of the electron coordinate only. The angles θ and ϕ now define the radius vectors of the electron from the center of mass. θ_k and ϕ_k give the final direction of motion of the photofragments in the space-fixed frame.

Using these wave functions, matrix elements of R appearing in Eq. (6), or, equivalently, the shift, width, and coupling parameters, can be obtained for the case of elliptically polarized light for any values of the magnetic quantum numbers. For example, in terms of the ellipticity parameters A and B the width of the states J_a,M_a after integration over all possible directions of fragmentation is given by

$$\Gamma_{M_a}=\left[A^2\left\{\frac{(J_a+M_a+1)^2(J_a+M_a+2)(J_a-M_a+1)}{(2J_a+1)(2J_a+2)(J_a+1)(2J_a+3)}+\frac{(J_a-M_a-1)(J_a-M_a)^2(J_a+M_a)}{2J_aJ_a(2J_a+1)(2J_a-1)}\right\}\right.$$
$$\left.+B^2\left\{\frac{(J_a-M_a+1)^2(J_a-M_a+2)(J_a+M_a+1)}{(2J_a+1)(2J_a+2)(J_a+1)(2J_a+3)}+\frac{(J_a+M_a-1)(J_a+M_a)^2(J_a-M_a)}{2J_aJ_a(2J_a+1)(2J_a-1)}\right\}\right]|D_{ca}|^2 \ . \tag{23}$$

Here the radial bound-free matrix elements D_{ca} involve the integrals over all coordinates except θ and ϕ and we have neglected the variation of the radial integrals with angular momentum in the continuum. Similarly the Raman coupling between (J_a,M_a) and (J_a,M_a+2) is given by

$$AB\left[\frac{\{(J_a+M_a+1)(J_a+M_a+2)(J_a-M_a)(J_a-M_a-1)\}^{1/2}}{(2J_a-1)(2J_a+3)}\right]F \ ,$$

where F involves integrals over all coordinates except θ and ϕ.

Thus it is clear that a resonant two-photon ionization or dissociation process from an arbitrary unpolarized angular momentum state caused by elliptically polarized radiation can be very complicated. Instead of dealing with the general case we will discuss the features of two-photon transitions to the continuum from an initial state $|G\rangle$ with $J_g=0$ by absorption of elliptically polarized radiation.

In this case, by absorption of a single photon of frequency ω the system can reach either a state $|A_{+1}\rangle$ with $J_a=1$ and $M_a=1$ or a state $|A_{-1}\rangle$ with $J_a=1$ and $M_a=-1$. Using the linear combination of $|A_{+1}\rangle$ and $|A_{-1}\rangle$ one can construct two orthogonal states $|U\rangle$ and $|V\rangle$,

$$|U\rangle=-A|A_{+1}\rangle+B|A_{-1}\rangle \ , \tag{24a}$$

$$|V\rangle=A|A_{+1}\rangle+B|A_{-1}\rangle \ , \tag{24b}$$

such that the transition from the initial state $|G\rangle$ to state $|V\rangle$ will be forbidden. Thus the state $|V\rangle$ becomes decoupled from the initial state. However, two-photon couplings between $|U\rangle$ and $|V\rangle$ exist and when $|U\rangle$ is

excited, state $|V\rangle$ may also become populated through two-photon coupling terms if the field is intense enough. The problem is thus reduced to that of a three-level system with the initial ground level connected to one intermediate resonant level by a dipole interaction and to the continuum by two-photon coupling. The two intermediate levels are each coupled to the continuum. They are also two photon (Raman) coupled to each other through continuum and discrete (if any) states. The matrix elements of U in terms of the roots of Eqs. (6) for a three-level system have been given by us earlier [13]. The special advantage of this change of basis is that with changes in the ellipticity parameter the resonant states are redefined so that one of them always remains decoupled from the ground state and all the simplifications for cases of linear and circular polarization follow in a natural way in the same space-fixed axes.

Thus for three states the set of equations (6) takes the form

$$\begin{aligned}&(x-\tilde{\delta}_0)G_{gg}-\tilde{\Omega}_1 G_{1g}=1\ ,\\ &-\tilde{\Omega}_1 G_{gg}+(x-\tilde{\delta}_1)G_{1g}-\tilde{F}_{12}G_{2g}=0\ ,\\ &-\tilde{F}_{21}G_{1g}+(x-\tilde{\delta}_2)G_{2g}=0\ .\end{aligned}\tag{25}$$

Here $x=z-E_g-f_g$ and $\tilde{\delta}_0$, $\tilde{\delta}_1$, and $\tilde{\delta}_2$ are interpreted as the complex detunings of the three states $|g\rangle$, $|1\rangle$, and $|2\rangle$, respectively,

$$\tilde{\delta}_0=-\frac{i}{2}\gamma_g\ ,\tag{26a}$$

$$\tilde{\delta}_k=\delta_k-\frac{i}{2}\Gamma_{a_k}\quad(k=1,2)\tag{26b}$$

and

$$\delta_k=E_k+F_k-E_g-f_g\ .\tag{26c}$$

$\tilde{\Omega}_1$ and $\tilde{F}_{12}$ are the complex effective couplings between these states calculated to the lowest nonvanishing orders using the pole approximation [12] for both the real and imaginary parts of the matrix elements of R,

$$\tilde{F}_{12}=\tilde{F}_{21}\equiv F_{12}-\frac{i}{2}\Gamma_{12}\tag{26d}$$

and

$$\tilde{\Omega}_1=V_{1g}\left[1-\frac{i}{q_1}\right]\tag{26e}$$

In terms of the three roots x_1, x_2, and x_3 of the characteristic equation, the matrix element of U is obtained as

$$\begin{aligned}U_{cg}(\varepsilon,t)=&\frac{S(x_1)e^{-ix_1t}}{(x_1-x_2)(x_1-x_3)(x_1-\varepsilon)}\\ &+\frac{S(x_2)e^{-ix_2t}}{(x_2-x_1)(x_2-x_3)(x_2-\varepsilon)}\\ &+\frac{S(x_3)e^{-ix_3t}}{(x_3-x_1)(x_3-x_2)(x_3-\varepsilon)}\\ &+\frac{S(\varepsilon)e^{-i\varepsilon t}}{(\varepsilon-x_1)(\varepsilon-x_2)(\varepsilon-x_3)}\end{aligned}\tag{27}$$

and

$$\begin{aligned}S(x)=&V_{c1}\tilde{\Omega}_1(x-\tilde{\delta}_2)+V_{c2}\tilde{\Omega}_1\tilde{F}_{21}\\ &+V_{cg}^{(2)}(x-\tilde{\delta}_1)(x-\tilde{\delta}_2)-V_{cg}^{(2)}\tilde{F}_{12}^2\ .\end{aligned}\tag{28}$$

Using the standard forms of the wave functions in Eqs. (22) and the interaction Hamiltonian from Eq. (1), the quantities γ_g, $\Gamma_{1,2}$, $F_{1,2}$, and q_1 in Eqs. (26) are obtained for the initial quantum numbers ($J_g=0$ and $M_g=0$) and the final continuum angular momentum states ($J=0,2$ and $M=0,\pm2$), in terms of ellipticity parameters A and B using the standard theorems for the integrals over the angular coordinates [14]. They can be expressed in terms of those for linearly ($\varepsilon=0$, i.e., $A=B=1/\sqrt{2}$) or circularly ($\varepsilon=45°$, i.e., $A=0$) polarized light denoted by the superscripts l and c, respectively. For initial $J_g=0$ these relations become

$$\gamma_g^3=\tfrac{2}{3}(1+2A^2B^2)\gamma_g^1=(1+2A^2B^2)\gamma_g^c\ ,\tag{29a}$$

$$\Gamma_1^e=\tfrac{2}{3}(1\pm2A^2B^2)\Gamma_a^1=(1\pm2A^2B^2)\Gamma_a^c\ ,\tag{29b}$$

$$F_1^e=\tfrac{2}{3}(1\pm2A^2B^2)F_a^l=(1\pm2A^2B^2)F_a^c\ ,\tag{29c}$$

$$q_1^e=\tfrac{3}{2}[1+2A^2B^2]^{-1}q^l=[1+2A^2B^2]^{-1}q^c\ ,\tag{29d}$$

$$\tilde{F}_2^e=\tfrac{2}{5}AB(A^2-B^2)\left[F_a^l-\frac{i}{2}\Gamma_a^l\right]\ ,\tag{29e}$$

$$D_{1g}^e=D_{ag}^1=D_{ag}^c\ ,\tag{29f}$$

$$f_g^e=f_g^l=f_g^c\ .\tag{29g}$$

The index e refers to elliptically polarized light.

PHOTOFRAGMENT ANGULAR DISTRIBUTION USING ELLIPTICALLY POLARIZED LIGHT

The proper way of obtaining the angular distribution in the photofragment spectrum is to use the outgoing wave-vector angle-(θ_k,ϕ_k) dependent matrix elements of V in the numerator of W in Eqs. (21)–(27). The roots in the denominator, as well as the width and shifts of the levels arising in the expression for W, must, however, be obtained by integrating over all possible directions of final motion. This is necessary to ensure that the integrations over all angles do reproduce the total transition rate and the angular distribution satisfy the very general constraint provided by Yang's theorem [15]. These points were made by Dixit and McKoy [16] and have been reemphasized in a recent paper by Dixit [17].

In the expression of photofragment spectra for elliptically polarized light, the numerator [Eq. (27)] contains the dissociation angle-dependent terms V_{c1}, V_{c2}, and $V_{cg}^{(2)}$. After the evaluation of Clebsch-Gordan coefficients the intensity-independent parts of these matrix elements are obtained. For an initial $J=0$ state the matrix elements V

become

$$V_{1c}=\frac{1}{\sqrt{3}}\left[\frac{1}{4\pi}\right]^{1/2}[2ABD^0_{00}e^{-i\delta_0}-2ABD^2_{00}e^{-i\delta_2}+\sqrt{6}A^2D^2_{20}e^{-i\delta_2}+\sqrt{6}B^2D^2_{-20}e^{-i\delta_2}]D_{ac}\ , \tag{30a}$$

$$V_{2c}=\frac{1}{\sqrt{3}}\left[\frac{1}{4\pi}\right]^{1/2}[(A^2-B^2)D^0_{00}e^{-i\delta_0}-(A^2-B^2)D^2_{00}e^{-i\delta_2}-\sqrt{6}ABD^2_{z0}e^{-i\delta_z}+\sqrt{6}ABD^2_{-20}e^{-i\delta_2}]D_{ac}\ , \tag{30b}$$

$$V^{(2)}_{cg}=\frac{1}{\sqrt{3}}\left[\frac{1}{4\pi}\right]^{1/2}\left[\frac{2}{\sqrt{3}}ABD^0_{00}e^{-i\delta_0}-\frac{2}{\sqrt{3}}ABD^2_{00}e^{-i\delta_2}+\sqrt{2}A^2D^2_{20}e^{-i\delta_2}+\sqrt{2}B^2D^2_{-20}e^{-i\delta_2}\right]D^{(2)}_{cg}\ . \tag{30c}$$

Here D_{ac} and $D^{(2)}_{cg}$ include both the intensity-dependent factor and the radial parts. δ_0 and δ_2 are phase shifts for $J=0$ and 2 partial waves in the continuum. $D^J_{M\Lambda}$ has been written for the rotation matrix elements $D^J_{M\Lambda}(\phi_k,\phi_k 0)$, where θ_k and ϕ_k are scattering angles of the fragments with respect to the propagation direction of radiation (Z). The major axis of the ellipse is defined as the X axis. Using these expressions in (28) $S(\varepsilon)$ becomes

$$S(\varepsilon)=\frac{1}{3\sqrt{4\pi}}\{[(A^2-B^2)H+2ABG]D^0_{00}e^{-1\delta_0}-[(A^2-B^2)H+2ABG]D^2_{00}e^{-i\delta_2}\}+\frac{2}{\sqrt{3}}\left[\frac{1}{4\pi}\right]^{1/2}\{[A^2G-ABH]D^2_{20}e^{-1\delta_2}+[B^2G+ABH]D^2_{-20}e^{-i\delta_2}\}\ , \tag{31}$$

where

$$G=D_{ac}V_{1g}(1-i/q_1)(\varepsilon-\delta_2)+D^{(2)}_{cg}(\varepsilon-\delta_1)(\varepsilon-\delta_2)-\tilde{F}^2_{12}\ , \tag{32a}$$

$$H=D_{ac}\tilde{F}_{21}V_{1g}(1-i/q_1)\ . \tag{32b}$$

Now defining

$$X=\left[\frac{A^2-B^2}{3}\right]H+\tfrac{2}{3}ABG\ , \tag{33a}$$

$$Y=\tfrac{2}{3}[A^2G-ABH]\ , \tag{33b}$$

$$Z=\tfrac{2}{3}[B^2G+ABH]\ , \tag{33c}$$

$$\delta_d=\delta_2-\delta_0\ , \tag{33d}$$

and taking the absolute squares of Eq. (27) using the addition theory of the rotation operator matrix elements [14], we can express, after much simplification, the angle-dependent numerator of the expression for angular distribution in terms of an expansion in Legendre polynomials in θ_k and a Fourier series in ϕ_k with θ_k-dependent coefficients with terms up to $\cos 4\phi_k$ and $\sin 4\phi_k$. The quantities X, Y, and Z entering the expression are complex numerical coefficients depending on intensity and molecular properties and have nothing to do with the space-fixed coordinates:

$$|S(\varepsilon)|^2=\left[|X|^2+\frac{|X|^2+|Y|^2+|Z|^2}{5}\right]+\tfrac{2}{7}[|X|^2-|Y|^2-|Z|^2-2|X|\cos\delta_d]P_2(\cos\theta_k)+\tfrac{1}{35}[8|X|^2+3|Y|^2+3|Z|^2]P_4(\cos\theta_k)$$
$$+\{\sqrt{\tfrac{3}{2}}|XY^*|\sin^2\theta_k\cos(2\phi_k+\delta_d+\kappa)+\sqrt{\tfrac{3}{2}}|XZ^*|\sin^2\theta_k\cos(2\phi_k-\delta_d+\psi)$$
$$+\tfrac{2}{7}\sqrt{\tfrac{3}{2}}|XY^*|\sin^2\theta_k\cos(2\phi_k+\kappa)+\tfrac{2}{7}\sqrt{\tfrac{3}{2}}|XZ^*|\sin^2\theta_k\cos(2\phi_k+\psi)$$
$$-\tfrac{3}{14}\sqrt{\tfrac{3}{2}}|XY^*|\sin^2\theta_k(7\cos^2\theta_k-1)\cos(2\phi_k+\kappa)$$
$$-\tfrac{3}{14}\sqrt{\tfrac{3}{2}}|XZ^*|\sin^2\theta_k(7\cos^2\theta_k-1)\cos(2\phi_k+\psi)+\tfrac{3}{4}|YZ^*|\sin^4\theta_k\cos(4\phi_k+\xi)\}\ , \tag{34}$$

where

$$XY^*=|XY^*|e^{i\kappa}\ ,\quad XZ^*=|XZ^*|e^{i\psi}\ ,\quad YZ^*=|YZ^*|e^{i\xi}\ . \tag{35}$$

Since the denominators in Eq. (27) are angle independent, Eq. (34) gives the expression for angular distribution of photofragments in the long-time limit within a constant factor for a given intensity, detuning, and the

kinetic energy of the fragments. Hence the distribution function $|S(\varepsilon)|^2$ is a function of both θ_k and ϕ_k and also depends on δ_d. The terms independent of ϕ_k constitute an expansion in terms of the Legendre polynomials in θ_k involving only terms up to P_4. The functional dependence on the azimuthal angle ϕ_k is expressed as a Fourier expansion involving $\cos 2\phi_k$, $\sin 2\phi_k$, $\cos 4\phi_k$, and $\sin 4\phi_k$ only with θ_k-dependent coefficients.

The normalized angular distribution after integrating over all ϕ_k gives

$$|S(\varepsilon)|^2 = 1 + a_2 P_2(\cos\theta_k) + a_4 P_4(\cos\theta_k) \ . \tag{36}$$

Here normalization means that the angle-integrated value of the numerator in Eq. (27) will be equal to unity. The coefficients are

$$a_2 = \frac{10}{7}\left[\frac{|X|^2(1-2\cos\delta_d) - |Y|^2 - |Z|^2}{6|X|^2 + |Y|^2 + |Z|^2}\right] \tag{37a}$$

and

$$a_4 = \tfrac{3}{7} \ . \tag{37b}$$

Both the ϕ_k-integrated distribution as well as the distribution on any one plane containing two axes will be intensity dependent for general polarizations. This follows from the fact that, for a general polarization, X, Y, and Z are complex intensity-dependent quantities which vary differently with variation in the intensity. For linear polarization $X = Y = Z$ and there is no intensity dependence of the angular distribution, as expected. For circular polarization also, only one of the two quantities Y or Z is nonvanishing while $X = 0$ and once again, the angular distribution is intensity independent. Further, since for circular polarization only the final angular momentum channel $J = 2$ is allowed, the angular distribution for circular polarization is independent of the phase shifts of the continuum wave functions also. Because of circular symmetry, the distribution for circular polarization will be ϕ_k independent and this fact also follows from Eq. (34). For general polarizations the distribution is symmetric about $\phi_k = 90°$ as well as about $\phi_k = 180°$.

RESULTS AND DISCUSSION

We denote by γ_g, Γ, and q the values of the ground-state and resonant state linewidths and the asymmetry parameter for linearly polarized light. These parameters for other ellipticities are calculated from these values with the help of Eq. (29). The line shift for linearly polarized light will be taken as $F = \Gamma$ always. All quantities with the dimension of energy, e.g., detuning, kinetic energy in the continuum, etc., will be measured in units of Γ for all polarizations. Time will be measured in units of $1/\Gamma$. The roots of the complex cubic equation (12) representing the positions and widths of the dressed states generated from $|g\rangle$, $|1\rangle$, and $|2\rangle$ by their interaction with the elliptically polarized radiation have been calculated by the method of successive iteration. When the magnitudes of the negative imaginary part of one of these roots is much smaller than those of the others, then twice the magnitude of that imaginary part defines dissociation rate at long times. For nearly equal roots the transition rate is not well defined and a time-dependent description of the dynamics is needed.

Figure 1 shows the transition rate against the detuning δ for $q = 5$, $\Gamma = 1$, and $V_{ag} = 0.1$. Here δ is the difference between the photon energy and the unshifted level energy for the resonant $J = 1$ state expressed in units of Γ. The ground-state two-photon width γ_g can be obtained from the relation $\gamma_g = 4D_{ag}^2/q^2\Gamma$. It was found that for this combination of parameters the transition rate is well defined for all ellipticity parameters, and we show the line shapes for $\phi = 0°$, 30°, and 45°. The two-photon coupling F_{12} vanishes for both linear and circular polarizations and the effect of this coupling on the dissociation rate is apparent near the Fano minimum for elliptic polarizations. The explanation of the relative shift of the Fano minimum for these three polarizations is the different level shifts in each case. For example, the position of minimum for $\phi = 0$ is given by $\delta + F' = q$ [Eq. (29c)]. The position of the minimum at $\phi = 45°$ is shifted from that for $\phi = 0°$ by $\frac{2}{3}\Gamma$, i.e., 0.666. The deep minimum appearing for linearly polarized radiation due to the destructive interference between the direct and sequential transition amplitudes is modified by the presence of the $|2\rangle$ state through which another pathway to the continuum is established. $|2\rangle$ is populated only by three-photon transitions from $|g\rangle$ and hence its effect only becomes apparent near the minimum where other pathways to the continuum are effectively blocked. The minimum for linearly polarized light becomes much shallower by an enhancement of the transition rate by six orders of magnitude near the minimum for elliptically polarized light. For circularly polarized light this enhancement is by about four orders of magnitude, which is solely due to geometrical factors. The small difference between the curves for the three polarizations away from the minimum also arises mainly due to geometrical factors. This also demonstrates how

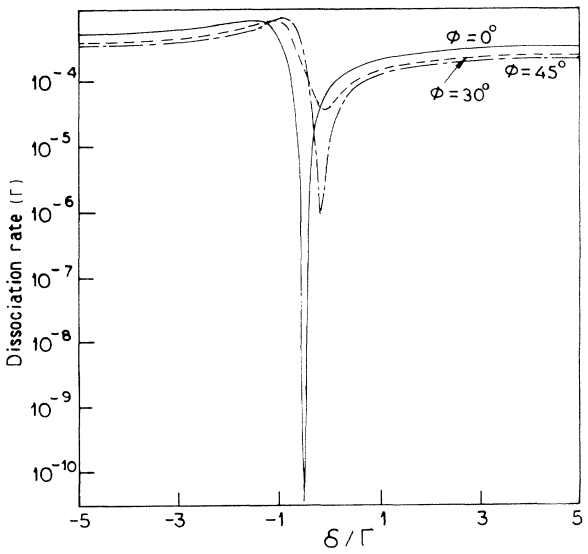

FIG. 1. Dissociation rate plotted against δ (in units of Γ) for $\phi = 0°$, 30°, and 45° using $\Gamma = 1$, $q = 5$, and $V_{ag} = 0.1$.

small changes in matrix elements can cause very large variations in observed quantities when destructive interference is involved. The positions of the maxima are slightly shifted for $\phi=45°$ and 30° from $\phi=0°$, though the peak heights are not very different for these polarizations.

Figures 2(a) and 2(b) show the transition probabilities at two different times $\Gamma t=1$ and 10, respectively, for the parameters $\Gamma=1$, $q=5$, and $V_{ag}=1$. Here the bound-bound coupling is as strong as the bound-free coupling and the transition rate is ill defined. Hence the transition probabilities are plotted. At the small value of time $\Gamma t=1$ [Fig. 2(a)] the probability shows similar variation with detuning at different polarizations. The maximum variation of polarization appears for higher negative detunings near $\delta=-3$ and the magnitude of $P(t)$ gradually

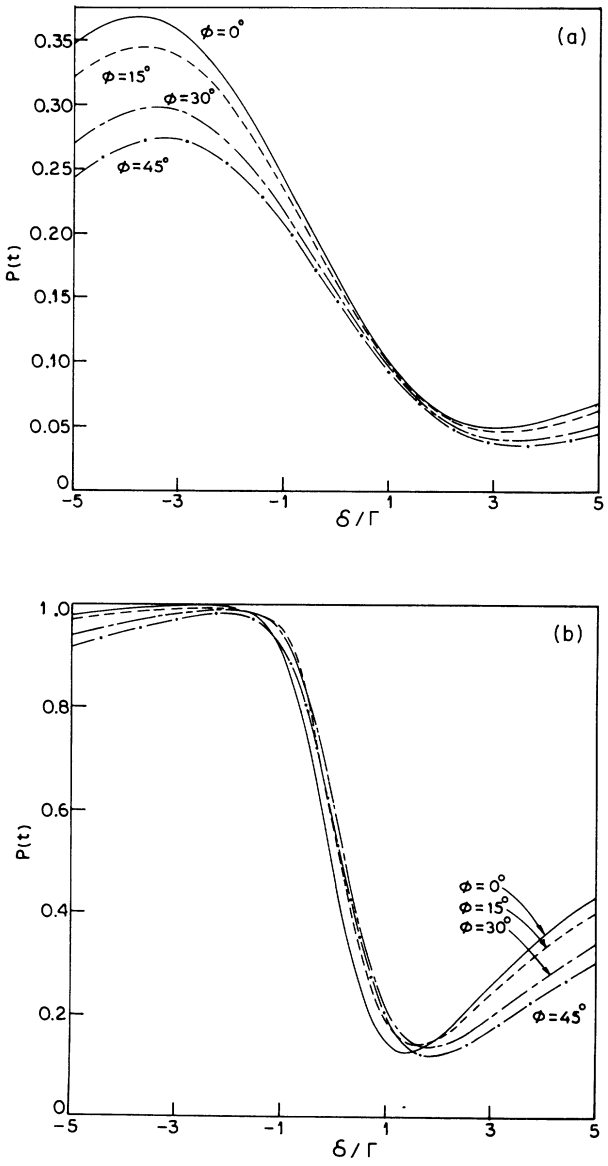

FIG. 2. (a) Dissociation probability $P(t)$ vs δ for $\phi=0°$, 15°, 30°, and 45° using $\Gamma=1$, $q=5$, and $V_{ag}=1$ at $\Gamma t=1$. (b) Same as (a) except at $\Gamma t=10$.

decreases with the change of polarization from linear to circular. Hence this difference is again mainly due to geometrical factors. This is to be expected, since the dominant coupling V_{ag} is not polarization dependent. Transition probabilities are found to be nearly equal for different ellipticity angles ($\phi=0°$, 15°, 30°, and 45°), near the region where one of the roots is much smaller than the others. The minima are obtained for these polarization angles near $\delta=3$. At larger detunings the probabilities slowly begin to increase and the curves differ from each other, although the magnitudes remain much smaller than those obtained at similar negative values of detunings. A similar behavior is seen at a longer time $\Gamma t=10$ in Fig. 2(b), where the probabilities have been plotted against detuning for the same four ellipticity parameters. At this time the probabilities $P(t)$ approach saturation for all polarizations at negative values of the detuning. The curves cross each other twice at intermediate values of δ, but both for large negative and positive detunings, the relative orders of the transition probabilities remain the same as that for short times. The positions of minima at $\phi=0°$ and 45° are at $\delta=1.2$ and 1.8, respectively, and those for $\phi=15°$ and 30° lie in between.

In Figs. 3(a) and 3(b) we have taken a value of bound-bound coupling V_{ag} larger than Γ. The values of the parameters used are $\Gamma=1$, $q=5$, and $V_{ag}=2$. We see that in Fig. 3(a), which has been drawn for linear polarization and a detuning $\delta=0$, the transition probability becomes almost constant after a steep initial increase, indicating a near trapping of the population in $|g\rangle$ and $|1\rangle$ states. When elliptically polarized light is used [Fig. 3(b)], the dissociation probability for the same detuning shows a slow increase at long times. This in another form again demonstrates that near-population trapping is effectively destroyed by two-photon couplings. The populations of states $|g\rangle$ and $|1\rangle$ exhibit oscillations with time. The maximum buildup of population in the state $|2\rangle$ is about 2% at intermediate times, but is much smaller compared with the population of state $|1\rangle$. Even smaller peaks appear in the population of state $|2\rangle$ at subsequent times, but these are not discernible on the scale of the figure.

In Figs. 4(a) and 4(b) the dissociation rates are plotted against the ellipticity angle ϕ for different values of detunings. Figure 4(a) shows the dissociation rate for $\delta=-1.5$, 0, and 1.5 using the values $\Gamma=1$, $q=5$, and $V_{ag}=0.1$. For $\delta=1.5$, the values of dissociation rate are magnified by a factor of 100 to represent them on the same scale. At this value of δ the dissociation rate goes through a deep minimum for $\phi=0°$, as seen from Fig. 1. For different values of detunings the behaviors of the dissociation rate with ellipticity angle ϕ are different. For $\delta=1.5$ the dissociation rate increases with ϕ and shows a maximum at $\phi=24°$, which is nearly 15 times larger than the value of this rate for $\phi=0°$. In the range $24° < \phi < 45°$ is again decreases to a small value. At $\delta=0$ the variation of dissociation rate with ϕ is similar to that at $\delta=1.5$, though the maximum dissociation rate at $\phi=28°$ is only 4.5 times larger than the minimum value at $\phi=0°$. At $\delta=-1.5$, however, the dissociation rate is maximum at $\phi=0°$ and decreases slowly up to about $\phi=10°$. For $\phi\cong 10°-40°$ dissociation rate decreases more rapidly with

ϕ and then becomes flat again near $\phi=45°$. The resultant variation of the dissociation rate for different detunings is a consequence of the variation of the parameters with the ellipticity angle which gives rise both to geometrical factors and two-photon coupling effects as discussed earlier. The second factor becomes significant near the minimum of the rate.

Figure 4(b) shows the variation of the dissociation rates with ϕ for $\delta=-2.4$, 0, and 2.4, but with the intensity reduced by a factor of 10. The parameters are related to the intensity I as $\Gamma \propto I$, $q \propto 1/I$, and $V_{ag} \propto \sqrt{I}$ and are changed accordingly. The magnitudes of the dissociation rates are now smaller compared to those in Fig. 4(a). At this intensity, the dissociation rate has a minimum for $\delta=2.4$. The variation of the dissociation rate with ellipticity angle ϕ at this detuning ($\delta=2.4$) shows a steep rise up to $\phi=8°$. There is an increase of the magnitude by four orders in this small range. For $\delta=0$ and -2.4 dissociation rates are much larger and show a slight monotonic increase and decrease with ϕ for $\delta=0$ and $\delta=-2.4$, respectively.

Figures 5(a) and 5(b) indicate the nature of evolution of the photofragment energy distribution by showing it at $\Gamma t=10$ and 100 for $\phi=0°$, 30°, and 45° and $\delta=0$ for two different sets of parameters as functions of ε $[=(E_c-E_G-2\hbar\omega)/\Gamma]$. The distribution obtained at small time ($\Gamma t=10$) in these figures shows different shapes for these three ellipticity angles. Figure 5(a) has been obtained for $\Gamma=1$, $q=5$, and $V_{ag}=1$. At $\Gamma t=10$ the distribution for $\phi=0°$ shows a number of peaks and

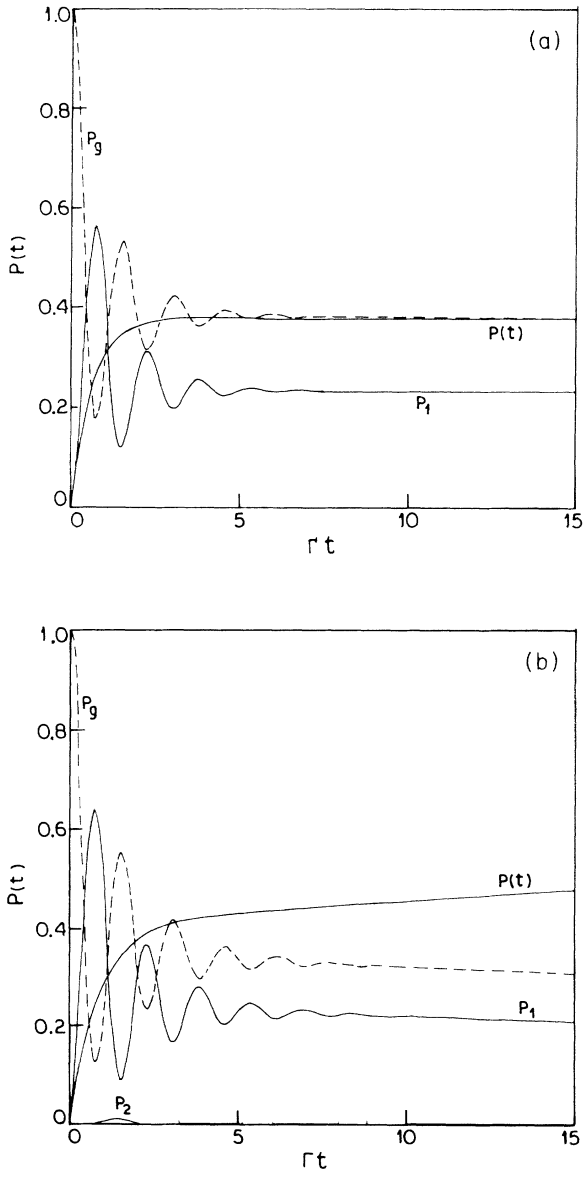

FIG. 3. (a) Dissociation probability $P(t)$ vs Γt for $\phi=0$ at $\delta=0$ and $\Gamma=1$, $q=5$, and $V_{ag}=2$. (b) Same as (a) except for $\phi=30°$.

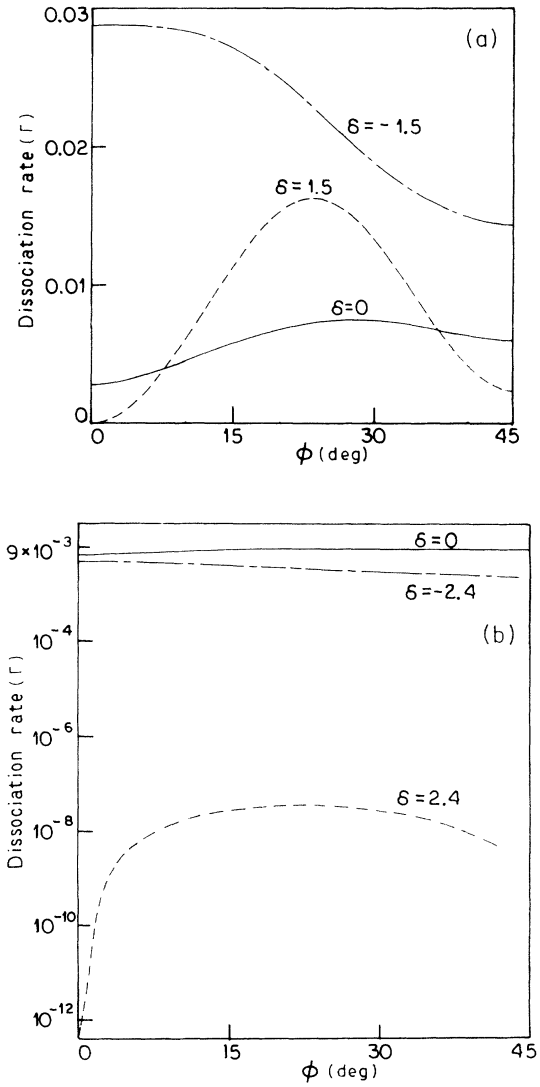

FIG. 4. (a) Dissociation rate plotted against ϕ at $\delta=-1.5$, 0, and 1.5 for $\Gamma=1$, $q=5$, and $V_{ag}=0.1$. The values for $\delta=1.5$ are magnified by a factor of 100. (b) Same as (a) except at $\delta=-2.4$, 0, and 2.4 and for the intensity reduced by a factor of 10.

the peak at $\varepsilon=-0.5$ is larger than the others. Similar types of distributions have been obtained at the same time ($\Gamma t=10$) for $\phi=30°$ and 45°. For $\phi=30°$, the peak at $\varepsilon=-0.75$ is much larger (3 times) than that near $\varepsilon=1.5$. For $\phi=45°$ the peak at $\varepsilon=-0.7$ is 1.5 times larger than that at $\varepsilon=1.5$. A number of peaks arise at a short time because all the roots of the secular equation contribute to the dissociation amplitude. The imaginary parts of two of the roots are nearly equal because the bound-bound coupling V_{ag} is equal to Γ. At a longer time ($\Gamma t=100$), a sharp peak arises at the same position as that of the larger peak for the shorter time ($\Gamma t=10$) for each ϕ. Also, at long times, an inelastic peak appears for each ϕ at the same position as that of the secondary peak observed at shorter time. This peak is roughly 100 times smaller than the sharp one, its height being slightly larger for $\phi=45°$. At long times, the major contribution comes from the smallest root only.

Figure 5(b) is drawn for the same values of Γ and q as in Fig. 5(a), but for $V_{ag}=2$ Fig. 5(b) has shapes very different from those presented in Fig. 5(a) for all the ϕ's. The shapes of the distributions obtained at $\Gamma t=10$ are drastically changed at the longer time $\Gamma t=100$. At $\Gamma t=10$, one large peak at $\varepsilon=2.5$ and a number of small peaks, with one of them at a negative value of ε and more prominent than the others, arise. At longer time ($\Gamma t=100$), only two peaks remain, one at the position of the large peak ($\varepsilon=2.5$) and the other at the position of the secondary peak observed at a short time. However, in this case, the peak at $\varepsilon=2.5$ remains much broader compared to the other one for each ϕ. The height of the narrower peak for $\phi=0°$ is nearly equal to the broader

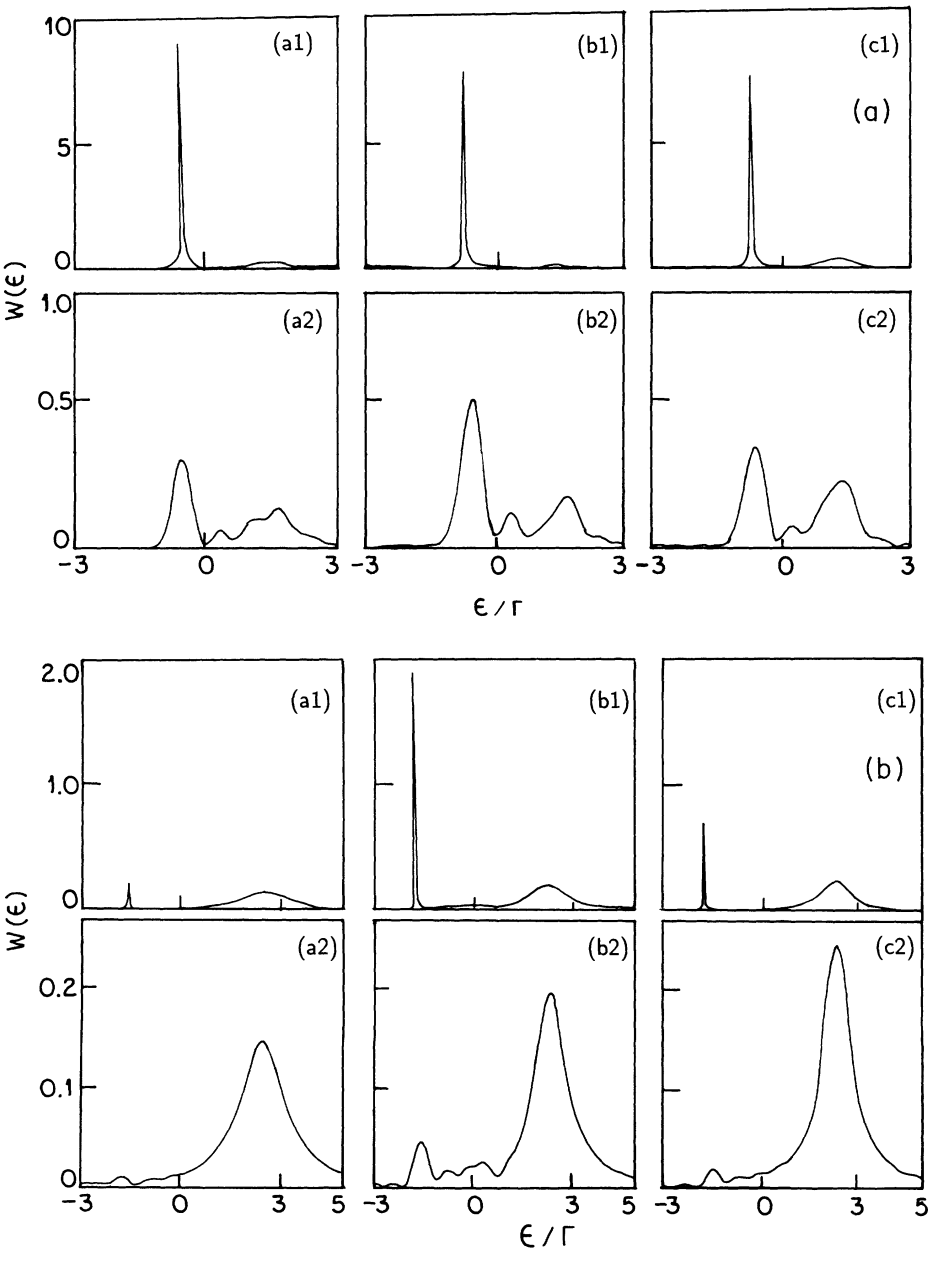

FIG. 5. (a) Kinetic-energy distribution W of the photofragments against ε for (a1) $\phi=0°$ and $\Gamma t=100$, (a2) $\phi=0°$ and $\Gamma t=10$, (b1) $\phi=30°$ and $\Gamma t=100$, (b2) $\phi=30°$ and $\Gamma t=10$, (c1) $\phi=45°$ and $\Gamma t=100$, and (c2) $\phi=45°$ and $\Gamma t=10$. In this figure $\Gamma=1$, $q=5$, and $V_{ag}=1$. (b) Same as (a) except for $\Gamma=1$, $q=5$, and $V_{ag}=2$.

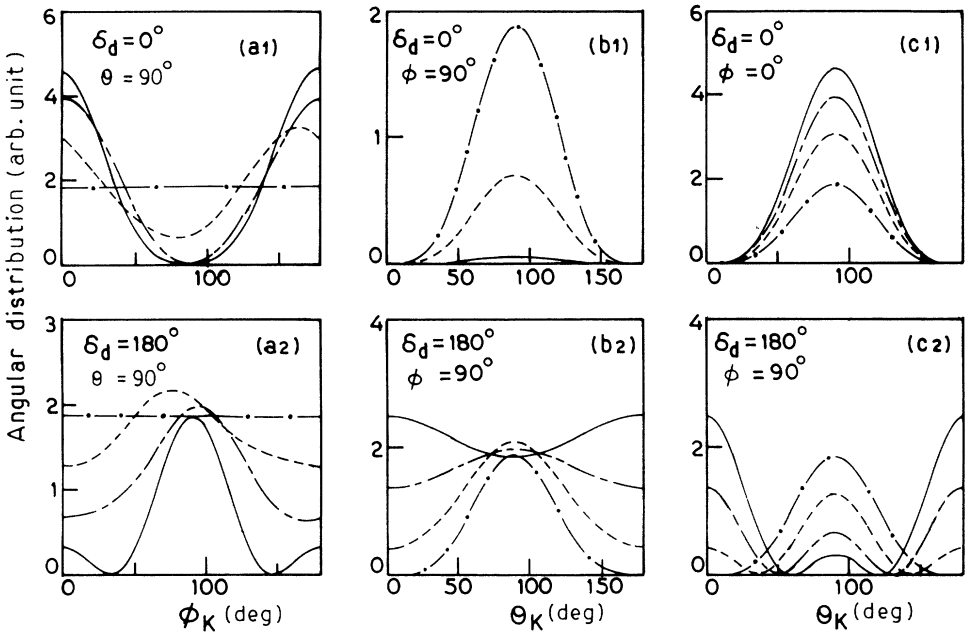

FIG. 6. Angular distribution of the photofragments for the parameters $\Gamma=1$, $q=5$, and $V_{ag}=0.1$ for $\delta_d=0°$ plotted against (a1) ϕ_k when $\theta_k=90°$ (in the XY plane), (b1) θ_k when $\phi_k=90°$ (in the YZ plane), and (c1) θ_k when $\phi_k=0°$ (in the XZ plane). For these figures $\delta_d=0$. (a2), (b2), and (c2) show the corresponding angular distributions for $\delta_d=180°$. The solid, long-dash–short-dashed, dashed and dot-dashed lines are for $\phi=0°$, 15°, 30°, and 45°, respectively.

peak at $\varepsilon=2.5$ but for $\phi=30°$ this height (at $\varepsilon=-1.75$) is about 10 times greater than that of the broader peak. For $\phi=45°$ the height of the narrower peak (at $\varepsilon=-1.75$) is 3 times greater than the other one.

The angular distributions of the photofragments in the XY plane ($\theta=90°$) has been plotted against the angle ϕ_k in Figs. 6(a1) and 6(a2) for the ellipticity angles $\phi=0°$, 15°, 30°, and 45° for a particular choice of parameters $\Gamma=1$, $q=5$, and $V_{ag}=0.1$. The two figures have been drawn for two values of the continuum phase shift difference δ_d between the $J=0$ and 2 wave functions. The upper curves are for $\delta_d=0°$, while the lower curves are for $\delta_d=180°$. In general, this distribution will depend on ε. We have taken $\delta=0$ for all polarizations, which means an exact resonance with the unshifted field-free level. With change in polarization, there will be a consequent change in the detuning from the shifted resonance state which enters into the expression for the distribution. However, for our choice, the peak of the photofragment spectrum will be very near $\varepsilon=0$ for all polarizations. We have plotted the distribution at this single value of ε, $\varepsilon=0$. It is to be noted that if we change ε and δ in the same way, keeping the intensity and polarization the same, the angular distribution does not change. For our choice of parameters the pattern of angular distribution is insensitive to the change in detuning which occurs due to polarization effects. This will not be true for considerably larger shift of the resonant level. This point will be discussed in more detail in connection with the intensity dependence of the angular distribution. From Figs. 6(a1) and 6(a2) we see that for linear polarizations, no fragments will be observed perpendicular to both the polarization direction and the propagation direction when the phase shifts for $J=0$ and 2 are the same. On the other hand, for a phase-shift difference of 180°, maximum fragmentation will occur in a direction perpendicular to the polarization direction in a plane perpendicular to the direction of propagation. For circular polarization, simply for reasons of symmetry, fragmentation arises in all directions in the XY plane equally and the magnitude is independent of δ_d, as mentioned previously. The case for other ellipticity angles are intermediate. For example, for $\phi=30°$, the minimum (maximum) in the XY plane will be slightly shifted from $\phi_k=90°$ for $\delta_d=0°$ (180°). For $\phi=15°$, the distribution shows a minimum (maximum) very close to $\phi_k=90°$ for $\delta_d=0°$ (180°), but this is much narrower compared with that for $\phi=0°$. The maximum (minimum) fragmentation is thus also nearly along the major axis of the ellipse. It should be mentioned that, in a recent work, Reid, Leahy, and Zare have shown how the use of different combinations of polarizations of two-photon fields in a resonant two-photon ionization process

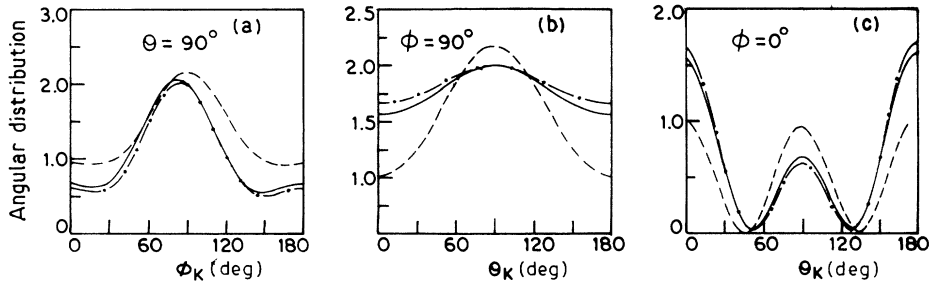

FIG. 7. Same as Fig. 6 except for $\delta_d=18°$ and $\phi=30°$ at exact resonance with shifted state $|1\rangle$ for intensities $I=10$ (dashed line), 1 (solid line), and 0.1 (dot-dashed line).

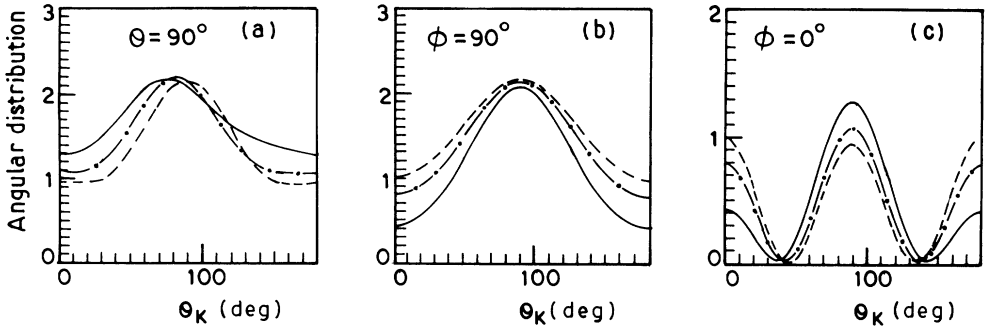

FIG. 8. Same as Fig. 7 except that the exact resonance is with the field-free $|U\rangle$ state.

lead, under certain circumstances, to the breaking of cylindrical symmetry in the angular distribution [18].

Figures 6(b1) and 6(b2) show the pattern of fragmentation in the YZ plane which is perpendicular to the major axis of the ellipse. In this plane $\phi_k=90°$ and the angular distributions have been plotted as functions of θ_k. For linearly polarized light, the angular distribution is very flat in this plane. Almost no fragmentation occurs for $\delta_d=0°$, but for $\delta_d=180°$ this is the preferred plane of fragmentation for linear polarizations. For most ellipticity angles, there will be a peak at $\theta_k=90°$ in the YZ plane for all values of δ_d. The sharpness of this peak will, however, be greatest for circularly polarized light.

The angular distribution in the XZ plane ($\phi_k=0°$), containing both the propagation direction and the major axis of the ellipse, have been shown as functions of θ_k in Figs. 6(c1) and 6(c2) for $\delta_d=0°$ and 180°, respectively. For $\delta_d=0°$ the pattern of the angular distribution in the XZ plane is the same as in the YZ plane. However, the peak at $\theta_k=90°$ is now sharpest for linearly polarized light. For $\delta_d=180°$ there are peaks both at $\theta_k=90°$ as well as $\theta_k=0°$ and 180° except for circularly polarized light. There are two zeros symmetrically located on each side of $\theta_k=90°$. The depth of the modulation decreases with increase in the ellipticity angle. From a three-peaked structure the pattern reduces gradually to that with a single peak as the polarization is gradually changed from linear to circular.

Figures 7 and 8 demonstrate the effect of change in laser intensity on the angular distribution. The distributions in the YZ, XY, and XZ plane have been plotted in (a), (b), and (c), respectively. δ_d has been taken to be equal to 180° and the ellipticity angle ϕ has been fixed at $\phi=30°$ in all cases. (No intensity dependence can occur for linear and circular polarizations within our approximations.) In Fig. 7, intensity effects have been demonstrated, always maintaining exact resonance, after taking into account the shift (which is equal to Γ) at different intensities. The distributions have been shown for $\varepsilon=0$. For $\Gamma=1$, $q=5$, and $V_{ag}=0.1$ we have arbitrarily defined the intensity to be unity. For any other intensity I, Γ has been changed by a factor of I, q by a factor of $1/I$, and V_{ag} by a factor of $I^{1/2}$. From Fig. 7(a) we see that there is not much difference in the angular distributions for $I=0.1$ and 1, but at higher intensity $I=10$, there is a shift of the maximum away from $\phi_k=90°$ and a broadening of the distribution in the XZ plane. In the XY plane the distribution becomes narrower with the peak height at $\theta_k=90°$ considerably exceeding the values at $\theta_k=0°$ and 180° for higher intensity. In the YZ plane the three peaks at $\theta_k=0°$, 90°, and 180° become more and more nearly equal in magnitude as the intensity is increased.

Figure 8 shows the angular distribution for the same choice of intensities and parameters as well as δ_d and ϕ, but with the frequency adjusted to an exact resonance with the field-free level, i.e., $\delta=0$. As can be seen, the curves for $I=10$ are now closer to those for $I=0.1$ than to those for $I=1$. This demonstrates the effect of detuning. Since the real frequency remains the same, the detuning of the bound-bound transition is considerably increased relative to the strength of the bound-bound coupling because the shift is proportional to intensity, but the bound-bound coupling increases only as the square root of intensity. Thus the effect of introducing additional detuning is to bring the shapes of the angular distributions closer to those for a lower intensity.

ACKNOWLEDGMENT

This work has been done as part of a project sponsored by the U.S.–India Fund.

[1] A. T. Georges and P. Lambropoulos, Adv. Electron. Electron Phys. **54**, 191 (1980); B. L. Beers and L. Armstrong, Jr., Phys. Rev. A **24**, 2247 (1975); P. Lambropoulos and P. Zoller, *ibid.* **24**, 379 (1981); Y. S. Kim and P. Lambropoulos, *ibid.* **29**, 3159 (1984); B. Datta and S. S. Bhattacharyya, J. Chem. Phys. **94**, 7779 (1991); **97**, 5941 (1992); J. Phys. B **26**, 921 (1993); S. Ganguly, K. Rai Dastidar, and T. K. Rai Dastidar, Phys. Rev. A **33**, 337 (1986); N. Sen, K. Rai Dastidar, and T. K. Rai Dastidar, *ibid.* **38**, 841 (1988); **40**, 735 (1989); S. N. Dixit and P. Lambropoulos, *ibid.* **27**, 861 (1983); S. N. Dixit and V. McKoy, J. Chem. Phys. **82**, 3546 (1985); H. Rudolph, D. L. Lynch, S. N. Dixit, and V. McKoy, *ibid.* **84**, 6657 (1986); X. Tang, A. Lyras, and P. Lambropoulos, J. Opt. Soc. Am. B **7**, 456 (1990); P. Lambropoulos and X. Tang, in *Atoms in Intense Laser Fields*, edited by M. Gavrilla (Academic, New York, 1992).

[2] B. W. Shore, *The Theory of Coherent Atomic Excitation*

(Wiley, New York, 1989), Vol. 2, Chaps. 20 and 21.
[3] S. Banerjee, M. K. Chakrabarti, S. S. Bhattacharyya, and S. Saha, J. Chem. Phys. **95**, 1608 (1991); **96**, 4974 (1992).
[4] B. Datta and S. S. Bhattacharyya, Phys. Rev. A **48**, 2153 (1993).
[5] R. G. Bray and M. Hochstrasser, Mol. Phys. **31**, 412 (1976); K. Chen and E. Yeung, J. Chem. Phys. **69**, 43 (1978); **72**, 4723 (1980).
[6] S. J. Smith and G. Leuchs, Adv. At. Mol. Phys. **24**, 157 (1987).
[7] J. S. Bakos, Phys. Rep. **31**, 209 (1977).
[8] P. E. Coleman and P. L. Knight, J. Phys. B **14**, 2139 (1981).
[9] A. M. Tumaikin and V. I. Yudin, Zh. Eksp. Teor. Fiz **98**, 81 (1990) [Sov. Phys. JETP **71**, 43 (1990)].
[10] M. L. Goldberger and K. M. Watson, *Collision Theory* (Wiley, New York, 1964), Chap. 8; F. H. M. Faisal, *Theory of Multiphoton Processes* (Plenum, New York, 1987), p. 179; C. Cohen-Tannoudji, J. Dupont-Roc, and G. Grynberg, *Atom-Photon Interactions* (Wiley, New York, 1992).
[11] M. Born and E. Wolf, *Principles of Optics* (Pergamon, New York, 1965).
[12] M. Crance, in *Multiphoton Ionization of Atoms,* edited by S. L. Chin and P. Lambropoulos (Academic, New York, 1984), p. 65.
[13] B. Datta and S. S. Bhattacharyya, J. Phys. B **26**, 921 (1993).
[14] R. N. Zare, *Angular Momentum* (Wiley, New York, 1988).
[15] C. N. Yang, Phys. Rev. **74**, 764 (1948).
[16] S. N. Dixit and V. McKoy, J. Chem. Phys. **80**, 5867 (1984).
[17] S. N. Dixit, Phys. Rev. A **42**, 6932 (1990).
[18] K. L. Reid, D. J. Leahy, and R. N. Zare, J. Chem. Phys. **95**, 1746 (1991); **95**, 1757 (1991).